

The CLASS blazar survey. I - selection criteria and radio properties

M. J. Marchā,¹ [★] A. Caccianiga,¹ I.W.A. Browne², N. Jackson,²

¹ CAAUL, Observatório Astronómico de Lisboa, Tapada da Ajuda, 1349-018 Lisboa, Portugal

² University of Manchester, Jodrell Bank Observatory, Macclesfield, Cheshire SK11 9DL, UK

arXiv:astro-ph/0108468v1 29 Aug 2001

ABSTRACT

This paper presents a new complete and well defined sample of Flat Spectrum Radio Sources (FSRS) selected from the CLASS survey with the further constraint of a bright ($\text{mag} \leq 17.5$) optical counterpart. The sample has been designed to produce a large number of low-luminosity blazars in order to test the current unifying models in the low luminosity regime. In this first paper the new sample is presented and the radio properties of the 325 sources contained therein discussed.

Key words: surveys - radio continuum: general - galaxies: active BL Lacertae objects: general

1 INTRODUCTION

The term *blazar* groups together two types of Active Galactic Nuclei (AGNs): the Flat Spectrum Radio Quasars (FSRQs) and the BL Lac objects. The former, which are thought to be the beamed cores of FR II radio galaxies (Urry & Padovani, 1995), are predominantly high luminosity sources which show strong and broad emission features in their spectra whereas the latter, usually associated with beamed cores of FR I radio galaxies (Urry & Padovani, 1995), are primarily low luminosity objects showing only weak or even absent emission features in their spectra. Despite this dichotomy in the type of optical spectra, and luminosity range, the 2 types of sources share a smooth non-thermal continuum extending from radio to the X-rays, as well as the same violent behavior such as the high degree of polarisation and variability.

Recent years have seen a proliferation of efforts in order to find a possible connection between the 2 types of blazars. The fact that no basic differences were observed between the ratios of core to extended radio luminosity and of X-rays to extended radio luminosity for BL Lacs and FSRQs, led Maraschi & Rovetti (1994) to propose that the 2 types of sources were basically similar, varying only in their global intrinsic power. Later, Ghisellini (1997) and Fossati et al. (1998) proposed that the intrinsic power was indeed the driving feature behind the uniting sequence, but this time with the consequence of shifting the peak of the Spectral Energy Distribution (SED). Indeed, as far as the synchrotron

component of the spectrum is concerned there seems to be a sequence in the frequency at which the peak of the emission occurs: low luminosity sources (i.e. the weakest BL Lacs) peak at high frequencies (X-ray), while the high luminosity objects (i.e. FSRQ) peak at low frequencies (infrared/sub-mm). The position of the peak frequency is thought to be related to the cooling rate of the electrons responsible for the emission (Ghisellini 1997).

With the aim of investigating the relationship between BL Lacs and other Flat Spectrum Radio Sources (FSRS), Marchā et al. (1996) selected a sample of low-luminosity, core-dominated radio sources with flux density greater than 200 mJy at 5 GHz. By selecting sources with flat ($\alpha < 0.5$, $S_\nu \propto \nu^{-\alpha}$) radio spectra between 1.4 and 5 GHz and bright ($V < 17$) counterparts, this 200 mJy sample was expected to yield a purely radio flux limited sample out to $z = 0.1$. The objective was to obtain a statistically well defined sample of low luminosity FSRS consisting predominantly of optically passive sources, ie, sources with weak emission features which could be identified with the beamed counterparts of FRI radio galaxies. Spectroscopic observations, however, found an optical diversity which is difficult to understand under the current unified schemes for radio-loud AGN in the low luminosity regime. Apart from the expected BL Lacs and galaxies with weak emission lines (PEGs for 'Passive Elliptical Galaxies'), the data also yielded an unexpectedly high percentage ($\sim 20\%$) of strong emission-line objects. Among these, 2 sources were of particular interest since they showed an unusual combination of BL Lac and quasar properties. This 'hybrid' behavior is demonstrated by their low luminosity, flat radio spectrum, a highly polarised optical

[★] E-mail: mmarcha@oal.ul.pt

continuum (Jackson & Marchā 1999), and broad emission lines.

Evidence for a sequence in the broadband properties of blazars is found through the multi-wavelength study of the sources in the 200 mJy sample. Making use of data from across the spectrum, Antón (2000) finds a correlation between optical type, and the frequency at which the synchrotron component peaks for the FSRS of the 200 mJy sample. Specifically, BL Lacs tend to have the highest peak frequency, and PEGs the lowest, whereas the 2 low luminosity blazars mentioned before seem to have intermediate peak frequencies.

The 200 mJy sample, however, is relatively small (containing ~ 60 objects) which implies that the number of sources falling within each category gives poor statistics. Hence, confirmation of these results based on a more extensive study is a goal worth pursuing. The ideal sample should not only be larger than the 200 mJy, but also extend itself to lower radio luminosities since the goal is to select a sizeable number of low-power, low-redshift blazars. A search through the literature reveals a few samples of FSRS, but none with the desired specifications. For instance, both the 1 Jy sample (Kühr et al. 1981) containing 518 sources with flux densities at 5 GHz $S_{5\text{GHz}} \geq 1$ Jy and $V \leq 20$, and the CJ-F sample (Taylor et al. 1996) containing 293 sources with $S_{4.85\text{GHz}} \geq 350$ mJy and without specified magnitude limit are samples of too high a flux density limit to be of interest for the purpose in mind. The only other sample of FSRS available in the literature is the DXRBS (Perlman et al. 1998) containing sources resulting from a cross correlation between the WGACAT (White, Giommi, & Angelini 1994) X-ray catalogue, and a number of radio catalogues publicly available. The sample contains 298 sources of which 106 new identifications just appeared in the literature (Landt et al. 2001). However, this sample is not specifically targeted at selecting low-power, low-redshift BL Lacs, something that constitutes one of the goals of the present work.

Given the current situation with the available samples of FSRS, it was decided that the cleanest approach would be to select a new sample following the criteria used for the 200 mJy, but this time making use of a deeper survey. The starting point was the CLASS survey (Cosmic Lens All Sky Survey, Myers et al. 2001). The resulting sample goes to a limiting flux density of 30 mJy at 5 GHz, i.e., roughly 6 times lower than the flux density limit of the 200 mJy sample. In this paper the selection criteria of this new sample are presented and its radio properties discussed, leaving the discussion of the optical properties to a forthcoming paper (Caccianiga et al.; submitted to MNRAS).

The paper is organised as follows. In the next section the radio survey from which the sample was selected is briefly discussed. This is followed by the definition of the selection criteria of the new sample. Finally the radio properties of the sample are discussed and the summary presented.

2 THE CLASS SURVEY

The CLASS survey is one of the deepest survey of flat spectrum radio sources available so far. The primary goal of this survey was the selection, in the radio band, of gravitational lenses to be used to estimate the cosmological parameters.

The CLASS statistical sample, which contains $\sim 11,600$ sources, has been defined by using the NVSS catalogue (Condon et al. 1998) at 1.4 GHz and the GB6 catalogue (Gregory et al. 1996) at 5GHz. These two surveys offer the advantage of a large and uniform sky coverage at relatively deep flux limits (about 2.5 mJy for the NVSS survey and about 25 mJy for the GB6). The CLASS catalogue is the result of a positional cross-correlation between the two catalogues with the further constraint of a flat $\alpha_{1.4}^{4.8} \leq 0.5$, spectral index.

Since the two catalogues have been produced with instruments having different resolutions (the NVSS beam has FWHM=45'' while the GB6 beam has FWHM $\sim 3.5'$), some sources are resolved in more components in the NVSS than in the GB6 catalogue where they appear as a unique entry. As a consequence, the 1.4 GHz flux will be systematically underestimated in these cases and the corresponding spectral index will be flatter. This effect will bring some unwanted steep spectrum sources in the sample. In order to reduce this problem, the positional cross-correlation has been done in such a way that all the NVSS flux within a radius of 70'' of the GB6 position was considered (Myers et al., in preparation).

However, this procedure will not eliminate completely the steep spectrum sources from the sample because the Green Bank beam is incapable of resolving sources on scales up to $\sim 3\text{-}4'$. Indeed, some of these large double or triple radio sources have been found in the catalogue (see section 4.1).

3 THE OPTICALLY BRIGHT SUBSAMPLE

The main goal of the work presented here is to select a sample of low-luminosity blazars. Given the typical absolute magnitudes of the radio galaxies (Browne & Marchā 1993) it is expected that all blazars with $z \leq 0.15$ will have $R \leq 17.5$ due to the presence of the host galaxy. Thus, the *optically bright sample* selected from the CLASS survey by imposing the optical limit $R < 17.5$ will contain as a subset a purely radio flux limited sample for redshift below 0.15.

The selection of this sample was done by using the Automated Plate Measuring machine facility (APM; www.ast.cam.ac.uk/~apmcat/). Since APM covers only high galactic latitudes ($|b^{II}| \geq 15^\circ - 20^\circ$), the only objects considered were those with $|b^{II}| \geq 20^\circ$, where the catalogue is virtually complete.

Although APM offers the unique possibility of an automatic search for the optical counterparts of entire catalogues containing a large number of sources, there are two main problems which have to be addressed when dealing with the automatic identification of optical counterparts:

- (i) Uncertainty on the optical position for optically bright ($R_{APM} \leq 15$) and extended objects.
- (ii) Uncertainty on the APM magnitude for extended objects.
- (iii) APM blending or fragmentation of sources.

In order to address the first problem, the distribution of the NVSS/APM positional offset has been studied in three different bins of magnitude: $R_{APM} < 12$, $12 \leq R_{APM} < 16$ and $16 \leq R_{APM} < 18$ (Fig. 1). Positional offsets up to 30''

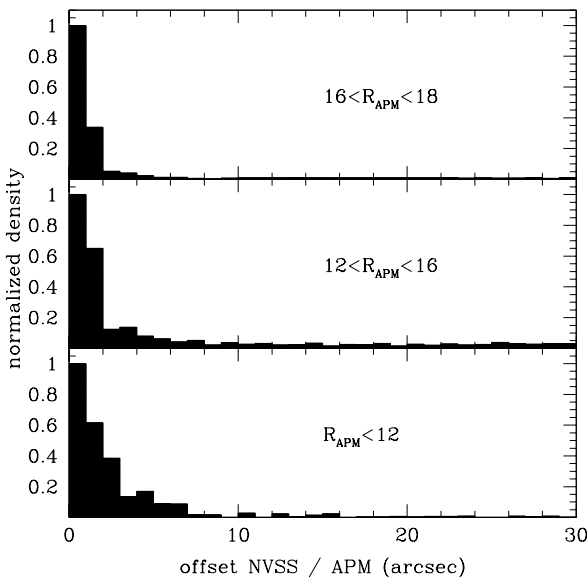


Figure 1. The normalized distribution of the offset between the CLASS and the APM positions in three different ranges of magnitudes. The plotted quantity is the number of sources in each bin divided by the bin area.

have been considered. The radius (b) of the circle that includes 95% of the optical counterparts has been computed by assuming that all the radio/optical matches with an offset larger than r_{max} are spurious. For the bins $12 \leq R_{APM} < 16$ and $16 \leq R_{APM} < 18$ an $r_{max}=15''$ was assumed, whereas for the brightest bin ($R_{APM} < 12$) an $r_{max}=20''$ was considered.

The resulting values of b are: $b=4''$ (for $16 \leq R_{APM} < 18$), $b=6''$ ($12 \leq R_{APM} < 16$) and $b=15''$ (for $R_{APM} < 12$).

The final list of sources was derived by keeping only the sources that have a radio/optical offset below b in the three magnitude intervals. In the case of the brightest bin ($R_{APM} \leq 12$), where the large positional tolerance can introduce some spurious radio/optical matches, the optical finding charts were visually inspected and the clear cases of wrong optical counterpart excluded.

The second issue to address in the optical identification process is the correction of the APM magnitudes. Due to the way the detection algorithm works, APM magnitudes for sources which are extended and brighter than ~ 17 can be systematically underestimated (Antón 2000). In particular, the APM red magnitudes (brighter than 15-16) appear systematically underestimated when compared with photometric magnitudes in R band (which is close to the band used for the POSS plates). This discrepancy appears more evident for extended objects (galaxies). However, besides this systematic discrepancy, a large dispersion (up to 2 magnitudes) is also observed. It was thus decided that an empirical correction should be applied to the red magnitude, in order to reduce these two problems. This correction has the following form (Antón 2000):

$$R = 7.235 + 0.605R_{APM} + 0.013\sigma_R$$

where R is the corrected R magnitude, R_{APM} is the observed APM red magnitude and σ_R gives the departure

from a Gaussian profile in units of σ (given in the APM output). The magnitude shown in Table 1 is this corrected magnitude.

Finally the problem of APM blending and fragmentation of sources was resolved by visual inspection of all of the finding charts. In this way it was possible to manually correct the few cases where the magnitude of a source was completely miscalculated due to the blending of 2 nearby objects.

In summary, the optically bright CLASS sample contains 325 sources which obey the following selection criteria:

- (i) $35^\circ \leq \delta \leq 75^\circ$
- (ii) $|b^{II}| \geq 20^\circ$
- (iii) $S_5 \geq 30$ mJy
- (iv) flat spectrum, i.e. $\alpha_{1.4}^{4.8} \leq 0.5$ ($S_\nu \propto \nu^{-\alpha}$)
- (v) APM red magnitude (corrected) ≤ 17.5

The complete sample of optically bright CLASS sources is presented in Table 1. The columns are: (1) - name, based on the GB6 position; (2) - the NVSS position (J2000); (3) - APM corrected red magnitude; (4) - the NVSS flux density (1.4 GHz). This is the sum of the fluxes of all the NVSS sources found within $70''$ from the GB6 position (in only 38 cases more than one NVSS component has been found); (5) - the GB6 flux density (4.8 GHz); (6) - VLA flux density at 8.4 GHz (“<” indicates upper limit for the detection); (7) - the spectral index between 1.4 and 4.8 GHz; (8) - the spectral index between 1.4 and 8.4 GHz (a “>” indicates an lower limit based on the detection limit in column 6); (9) - a flag indicating whether the source has been re-classified as steep, between 1.4 and 4.8 GHz on the basis of a re-analysis of the NVSS map. The corrected values of $\alpha_{1.4}^{4.8}$ are reported in parenthesis (see the next section for details).

4 RADIO PROPERTIES

The primary goal of this work is the selection of a sample of blazars, i.e. core-dominated, flat radio spectrum sources. However, the simple cross-correlation between the NVSS and the GB6 catalogue and the subsequent constraint on the radio spectral index can select some objects which are not truly FSRS and/or core-dominated sources. Hence, all additional available information to check the spectral indices and the radio morphology of the sources contained in the sample was considered. Specifically, the following pieces of information have been used:

- **VLA snap-shots at 8.4 GHz.** The entire CLASS catalogue has been observed at 8.4 GHz with VLA in A-configuration. Except for few (15) sources not detected at this frequency there is a flux density and a position at 8.4 GHz for 95% of the sources in the optically bright CLASS sample.

- **FIRST data.** The FIRST survey (Becker et al. 1995, White et al. 1997) is made at 1.4 GHz with VLA in B configuration which is a good compromise between resolution (beam $\sim 4''$) and sensitivity to extended emission (largest angular scale $\theta_{LAS} \sim 100''$). Hence, it is ideal to estimate the compactness parameter for the CLASS sources. About 50% of the sources in the sample fall in the region of sky covered by the FIRST survey.

Table 1. The CLASS bright sample (continued on the next page)

name	Position (J2000)	R mag	S _{1.4} (mJy)	S _{4.8} (mJy)	S _{8.4} (mJy)	$\alpha_{1.4}^{4.8}$	$\alpha_{1.4}^{8.4}$	flag
GB6J001450+385512	00 14 52.82 +38 55 19.3	17.00	48	47	28	0.02	0.30	
GB6J002538+400830	00 25 38.19 +40 08 42.3	15.23	37	32	19	0.12	0.37	
GB6J005529+354443	00 55 30.56 +35 44 35.4	17.00	49	32	27	0.35	0.33	
GB6J011216+381910	01 12 18.07 +38 18 56.9	17.28	58	52	126	0.09	-0.43	
GB6J011920+385253	01 19 20.13 +38 53 07.4	15.27	99	69	23	0.29	0.81	s (0.63)
GB6J012626+395406	01 26 25.82 +39 54 13.1	16.31	175	95	<2	0.50	>2.50	
GB6J013631+390623	01 36 32.43 +39 05 59.4	16.38	61	49	42	0.17	0.20	
GB6J014156+392325	01 41 57.67 +39 23 29.1	14.42	117	80	69	0.31	0.29	
GB6J015451+362746	01 54 51.59 +36 27 45.9	15.28	234	154	69	0.34	0.68	
GB6J020405+400512	02 04 05.16 +40 05 03.4	15.79	49	103	136	-0.60	-0.57	
GB6J021625+400101	02 16 24.55 +40 00 35.9	14.39	42	49	36	-0.12	0.09	
GB6J022526+371029	02 25 27.29 +37 10 27.9	14.01	197	137	167	0.29	0.09	
GB6J024621+353634	02 46 21.05 +35 36 38.0	17.50	190	108	128	0.46	0.22	
GB6J025359+362539	02 54 00.03 +36 25 51.5	12.39	83	63	53	0.22	0.25	
GB6J055253+724045	05 52 53.00 +72 40 45.5	17.37	508	385	256	0.23	0.38	
GB6J061641+663024	06 16 42.13 +66 30 24.1	13.43	288	174	126	0.41	0.46	
GB6J064204+675834	06 42 04.23 +67 58 35.6	17.03	193	488	419	-0.75	-0.43	
GB6J065010+605001	06 50 08.63 +60 50 44.7	12.38	63	44	25	0.30	0.52	
GB6J065422+504223	06 54 22.13 +50 42 23.5	16.13	198	136	305	0.30	-0.24	
GB6J065648+560258	06 56 47.58 +56 03 09.2	16.00	56	67	59	-0.14	-0.03	
GB6J065817+501641	06 58 18.49 +50 16 14.9	16.00	47	30	7	0.36	1.06	s (0.90)
GB6J070105+693634	07 01 06.53 +69 36 29.5	17.36	484	314	252	0.35	0.36	
GB6J070506+421457	07 05 07.17 +42 14 50.1	14.50	47	32	4	0.32	1.38	
GB6J070648+592327	07 06 49.54 +59 23 14.7	16.31	51	49	34	0.04	0.23	
GB6J070904+483659	07 09 07.83 +48 36 53.2	12.57	376	259	86	0.30	0.82	s (0.87)
GB6J070932+501056	07 09 34.27 +50 10 56.4	12.30	121	126	167	-0.03	-0.18	
GB6J071044+422053	07 10 44.30 +42 20 54.7	17.47	335	236	216	0.28	0.25	
GB6J071045+473203	07 10 46.16 +47 32 11.2	15.10	1019	984	620	0.03	0.28	
GB6J071433+740811	07 14 35.93 +74 08 09.7	17.30	116	216	134	-0.50	-0.08	
GB6J071510+452554	07 15 10.01 +45 25 55.5	14.51	76	98	90	-0.21	-0.09	
GB6J071547+413926	07 15 42.94 +41 39 23.5	16.15	104	56	12	0.50	1.20	
GB6J072028+370647	07 20 28.77 +37 06 45.2	16.95	13	36	37	-0.86	-0.61	
GB6J072151+712036	07 21 53.10 +71 20 36.7	15.96	727	859	594	-0.14	0.11	
GB6J072403+535121	07 24 05.73 +53 51 10.0	17.50	18	30	18	-0.43	-0.01	
GB6J072849+570124	07 28 49.59 +57 01 22.8	16.67	488	387	644	0.19	-0.15	
GB6J073328+351532	07 33 29.58 +35 15 42.4	16.80	102	70	34	0.31	0.61	
GB6J073502+475011	07 35 02.25 +47 50 07.9	17.45	405	511	460	-0.19	-0.07	
GB6J073654+653603	07 36 48.44 +65 36 41.5	8.93	57	51	<2	0.09	>1.87	s (0.82)
GB6J073728+594106	07 37 30.08 +59 41 03.4	13.69	561	370	248	0.34	0.46	
GB6J073758+643048	07 37 58.98 +64 30 43.4	17.13	417	251	239	0.41	0.31	
GB6J073933+495449	07 39 34.91 +49 54 39.0	16.11	101	55	48	0.49	0.42	
GB6J074904+451027	07 49 06.41 +45 10 33.8	17.14	159	113	43	0.28	0.73	
GB6J075038+654114	07 50 34.51 +65 41 23.4	16.95	32	52	27	-0.39	0.10	s (0.68)
GB6J080036+501047	08 00 36.03 +50 10 44.1	17.32	111	63	38	0.46	0.60	
GB6J080053+392433	08 00 53.56 +39 24 40.8	13.31	56	47	4	0.13	1.41	s (0.97)
GB6J080132+473624	08 01 31.88 +47 36 16.9	16.64	77	65	59	0.14	0.15	s (0.76)
GB6J080346+655424	08 03 47.78 +65 54 33.0	17.40	75	55	40	0.25	0.35	
GB6J080624+593059	08 06 25.94 +59 31 06.8	17.28	61	38	61	0.38	0.00	
GB6J080839+495033	08 08 39.74 +49 50 36.1	17.50	1115	1315	880	-0.13	0.13	
GB6J080949+521856	08 09 49.23 +52 18 58.1	15.69	183	184	154	-0.01	0.10	
GB6J081245+650843	08 12 41.08 +65 09 11.2	17.20	31	35	37	-0.10	-0.10	
GB6J081622+573858	08 16 22.68 +57 39 09.2	17.44	100	64	92	0.36	0.05	
GB6J082154+503136	08 21 53.77 +50 31 19.3	17.32	59	53	33	0.09	0.33	
GB6J082437+405712	08 24 38.88 +40 57 07.9	17.36	178	138	93	0.21	0.36	
GB6J083055+540041	08 31 00.36 +54 00 24.4	15.27	17	40	41	-0.71	-0.50	
GB6J083140+460800	08 31 39.80 +46 08 00.2	16.17	132	98	87	0.24	0.23	
GB6J083411+580318	08 34 11.06 +58 03 21.4	15.72	58	57	33	0.01	0.31	
GB6J083455+553430	08 34 54.91 +55 34 21.0	17.18	8284	5740	3234	0.30	0.52	
GB6J083901+401608	08 39 03.22 +40 15 46.6	16.81	46	34	19	0.25	0.50	
GB6J084124+705345	08 41 24.46 +70 53 41.4	17.31	3824	2342	1746	0.40	0.44	
GB6J084215+452547	08 42 15.43 +45 25 43.0	17.23	75	54	53	0.26	0.19	
GB6J084241+391100	08 42 41.78 +39 10 53.1	16.47	56	33	<2	0.42	>1.86	

Table 1 – continued

name	Position (J2000)	R mag	S _{1.4} (mJy)	S _{4.8} (mJy)	S _{8.4} (mJy)	$\alpha_{1.4}^{4.8}$	$\alpha_{1.4}^{8.4}$	flag
GB6J084352+374232	08 43 52.68 +37 42 27.0	17.10	104	61	45	0.43	0.47	
GB6J084356+510522	08 43 59.09 +51 05 25.5	16.16	201	116	44	0.45	0.85	s (0.57)
GB6J085005+403610	08 50 04.76 +40 36 07.4	17.29	133	110	144	0.15	-0.05	
GB6J085008+593054	08 50 10.00 +59 31 17.6	16.54	19	37	32	-0.52	-0.28	
GB6J085317+682824	08 53 19.15 +68 28 17.3	12.07	293	183	58	0.38	0.90	
GB6J085416+532731	08 54 17.56 +53 27 35.6	17.32	25	32	15	-0.20	0.29	
GB6J085449+621900	08 54 50.51 +62 18 50.5	17.44	388	215	317	0.48	0.11	
GB6J090536+470603	09 05 36.56 +47 05 46.5	17.10	102	86	63	0.14	0.27	
GB6J090615+463633	09 06 15.58 +46 36 19.0	16.65	291	159	206	0.49	0.19	
GB6J090643+710018	09 06 43.70 +71 00 30.2	16.46	55	31	15	0.46	0.72	
GB6J090650+412426	09 06 52.78 +41 24 29.1	14.52	54	65	81	-0.16	-0.23	
GB6J090757+493558	09 07 56.36 +49 35 48.3	15.00	43	36	28	0.14	0.24	
GB6J092230+710926	09 22 30.09 +71 09 36.3	17.28	83	83	56	0.00	0.22	
GB6J092914+501323	09 29 15.53 +50 13 35.5	17.30	523	544	747	-0.03	-0.20	
GB6J092932+625637	09 29 35.49 +62 56 59.1	15.34	56	33	15	0.42	0.73	
GB6J093254+673654	09 32 53.91 +67 37 07.0	12.16	238	131	28	0.48	1.19	
GB6J093737+723106	09 37 31.93 +72 30 55.2	16.44	26	39	35	-0.34	-0.17	
GB6J094319+361447	09 43 19.16 +36 14 52.2	12.94	75	81	335	-0.06	-0.83	
GB6J094542+575739	09 45 42.29 +57 57 46.2	16.87	125	92	69	0.25	0.33	
GB6J094557+461907	09 45 57.17 +46 19 18.6	16.74	27	31	57	-0.11	-0.42	
GB6J094614+581932	09 46 14.92 +58 19 34.5	16.23	87	56	12	0.35	1.10	
GB6J094832+553538	09 48 32.03 +55 35 35.6	15.78	31	34	22	-0.07	0.19	
GB6J095227+504837	09 52 27.15 +50 48 50.2	17.44	89	104	189	-0.12	-0.42	
GB6J095301+720231	09 52 58.29 +72 02 41.2	16.42	110	62	13	0.46	1.19	
GB6J095531+690357	09 55 33.28 +69 03 55.0	7.89	89	98	97	-0.08	-0.05	
GB6J095552+694047	09 55 51.88 +69 40 46.1	9.00	6437	3796	49	0.43	2.72	
GB6J095736+552258	09 57 38.18 +55 22 57.4	17.21	3080	2015	1498	0.34	0.40	
GB6J095847+653405	09 58 47.22 +65 33 54.3	16.58	730	1125	1224	-0.35	-0.29	
GB6J100055+533158	10 00 54.58 +53 32 05.5	17.39	109	72	28	0.34	0.76	
GB6J100308+681313	10 03 06.65 +68 13 17.4	16.25	103	86	64	0.15	0.27	
GB6J100712+502346	10 07 10.42 +50 23 55.8	16.53	31	34	24	-0.08	0.14	
GB6J100724+580201	10 07 24.89 +58 02 03.8	17.50	186	135	85	0.26	0.44	
GB6J101028+413230	10 10 27.63 +41 32 36.6	16.88	499	854	449	-0.44	0.06	
GB6J101244+423009	10 12 44.22 +42 29 56.7	17.40	80	46	41	0.44	0.37	
GB6J101504+492606	10 15 04.13 +49 26 01.1	16.67	378	299	252	0.19	0.23	
GB6J101859+591126	10 18 58.61 +59 11 27.9	17.26	98	76	61	0.21	0.26	
GB6J102310+394759	10 23 11.60 +39 48 17.2	17.32	1123	789	779	0.29	0.20	
GB6J102521+372641	10 25 23.42 +37 26 50.3	14.46	64	35	7	0.49	1.24	
GB6J102632+750501	10 26 30.53 +75 05 17.1	17.50	113	83	42	0.25	0.55	
GB6J103053+411300	10 30 53.56 +41 13 15.0	14.42	51	51	54	0.00	-0.03	s? (0.65)
GB6J103118+505350	10 31 18.51 +50 53 36.9	16.76	38	34	32	0.09	0.09	
GB6J103123+744158	10 31 22.57 +74 41 58.2	17.00	218	250	103	-0.11	0.42	
GB6J103318+422228	10 33 18.23 +42 22 37.2	17.34	46	34	16	0.24	0.58	
GB6J103550+375646	10 35 51.25 +37 56 41.3	17.44	53	34	54	0.36	-0.01	
GB6J103653+444832	10 36 52.95 +44 48 18.6	17.31	42	66	70	-0.37	-0.29	
GB6J103742+571158	10 37 44.28 +57 11 56.4	17.37	72	126	82	-0.46	-0.07	
GB6J103951+405557	10 39 51.04 +40 55 41.8	16.17	29	48	36	-0.42	-0.13	
GB6J104630+544953	10 46 28.73 +54 49 45.3	16.85	82	77	43	0.05	0.36	
GB6J104910+373742	10 49 09.82 +37 37 59.7	17.20	53	30	15	0.47	0.71	
GB6J105115+464439	10 51 15.97 +46 44 17.7	17.48	321	270	200	0.14	0.26	
GB6J105203+424203	10 52 04.15 +42 41 53.3	16.96	97	70	48	0.26	0.39	
GB6J105344+493006	10 53 44.02 +49 29 55.2	15.72	65	59	40	0.07	0.27	
GB6J105349+402337	10 53 49.14 +40 23 52.0	15.31	73	42	8	0.45	1.24	s (0.72)
GB6J105430+385500	10 54 31.80 +38 55 21.6	17.25	62	56	17	0.08	0.72	
GB6J105730+405631	10 57 31.12 +40 56 46.5	11.71	45	31	14	0.30	0.65	
GB6J105837+562817	10 58 37.71 +56 28 11.8	16.11	229	247	189	-0.06	0.11	
GB6J110147+722536	11 01 48.52 +72 25 37.4	17.42	1246	858	366	0.30	0.68	
GB6J110242+594132	11 02 42.65 +59 41 19.7	17.37	352	249	177	0.28	0.38	
GB6J110428+381228	11 04 27.42 +38 12 32.9	13.30	816	723	631	0.10	0.14	
GB6J110508+465311	11 05 07.05 +46 53 18.9	17.15	60	44	35	0.25	0.30	
GB6J110552+394649	11 05 53.69 +39 46 55.1	17.00	45	53	44	-0.13	0.01	
GB6J110657+603345	11 06 56.76 +60 34 02.4	16.54	33	31	28	0.04	0.09	

Table 1 – continued

name	Position (J2000)	R mag	S _{1.4} (mJy)	S _{4.8} (mJy)	S _{8.4} (mJy)	α _{1.4} ^{4.8}	α _{1.4} ^{8.4}	flag
GB6J110939+383046	11 09 39.19 +38 31 21.5	17.00	19	58	79	-0.93	-0.81	
GB6J111106+522751	11 11 05.75 +52 27 49.6	17.35	116	74	36	0.36	0.65	
GB6J111206+352707	11 12 08.06 +35 27 06.8	12.99	64	49	121	0.22	-0.36	
GB6J111309+401827	11 13 05.93 +40 17 32.8	15.00	13	45	19	-0.99	-0.20	s? (1.2)
GB6J111903+602832	11 19 04.13 +60 28 43.3	16.01	60	33	<2	0.49	>1.90	
GB6J111912+623938	11 19 16.56 +62 39 26.6	15.50	47	43	45	0.06	0.02	
GB6J111914+600459	11 19 13.90 +60 04 55.9	17.31	264	170	126	0.36	0.41	
GB6J112047+421206	11 20 48.06 +42 12 14.3	17.28	24	30	27	-0.18	-0.06	
GB6J112157+431459	11 21 56.66 +43 14 58.8	17.29	49	37	23	0.22	0.42	
GB6J112413+513350	11 24 13.14 +51 33 50.1	17.01	55	39	31	0.28	0.32	
GB6J112832+583322	11 28 32.61 +58 33 46.8	11.80	678	392	30	0.44	1.74	
GB6J113626+700931	11 36 26.48 +70 09 25.8	13.91	340	267	213	0.20	0.26	
GB6J113629+673707	11 36 29.92 +67 37 06.0	16.65	46	47	37	-0.02	0.12	
GB6J114047+462207	11 40 47.91 +46 22 04.0	16.02	99	54	22	0.49	0.84	
GB6J114115+595309	11 41 16.00 +59 53 09.2	14.24	119	147	106	-0.17	0.06	
GB6J114300+730413	11 43 04.73 +73 04 09.3	16.90	49	32	6	0.34	1.17	
GB6J114312+612214	11 43 12.10 +61 22 11.1	17.49	84	94	99	-0.09	-0.09	
GB6J114722+350109	11 47 22.14 +35 01 07.3	16.00	638	669	499	-0.04	0.14	
GB6J114850+592459	11 48 50.42 +59 24 57.3	14.15	482	566	521	-0.13	-0.04	
GB6J114856+525432	11 48 56.63 +52 54 25.7	16.74	93	288	597	-0.91	-1.04	
GB6J114959+552832	11 50 00.15 +55 28 21.8	16.82	153	83	70	0.50	0.44	
GB6J115037+653916	11 50 34.48 +65 39 28.8	17.08	78	60	49	0.21	0.26	
GB6J115126+585913	11 51 24.66 +58 59 18.6	17.41	185	131	102	0.28	0.33	
GB6J115757+552713	11 57 56.14 +55 27 12.6	11.47	101	88	157	0.12	-0.24	
GB6J120209+444452	12 02 08.43 +44 44 20.8	17.47	106	69	54	0.35	0.38	
GB6J120304+603130	12 03 03.55 +60 31 19.4	16.00	191	182	191	0.04	0.00	
GB6J120328+480316	12 03 29.92 +48 03 13.7	17.17	63	164	415	-0.77	-1.05	
GB6J120334+451050	12 03 35.49 +45 10 49.8	17.46	39	43	89	-0.08	-0.46	
GB6J120856+464112	12 08 55.57 +46 41 13.7	16.16	65	62	32	0.04	0.39	s (0.86)
GB6J120922+411938	12 09 22.82 +41 19 41.1	17.12	274	459	485	-0.42	-0.32	
GB6J121008+355224	12 10 08.05 +35 52 42.4	15.41	26	44	39	-0.44	-0.23	
GB6J121108+503000	12 11 11.37 +50 29 44.0	12.15	5	60	15	-1.97	-0.58	
GB6J121331+504446	12 13 29.28 +50 44 30.3	12.51	97	86	61	0.10	0.26	
GB6J121510+462710	12 15 09.99 +46 27 15.9	17.13	272	168	229	0.39	0.10	
GB6J121541+361924	12 15 39.98 +36 19 26.5	15.32	35	32	<2	0.07	>1.59	
GB6J121558+354313	12 15 59.38 +35 43 02.5	17.27	55	30	1	0.48	2.04	
GB6J121736+515502	12 17 36.72 +51 55 10.8	17.04	85	61	33	0.27	0.53	
GB6J122208+581427	12 22 09.40 +58 14 21.5	16.89	52	51	35	0.02	0.22	
GB6J122306+582659	12 23 02.04 +58 26 40.7	11.97	134	81	27	0.41	0.89	
GB6J122405+500130	12 24 09.92 +50 01 56.7	17.39	47	31	20	0.34	0.48	
GB6J123012+470031	12 30 11.80 +47 00 23.0	13.04	94	73	51	0.21	0.34	
GB6J123132+641421	12 31 31.34 +64 14 19.4	16.47	59	36	44	0.40	0.16	
GB6J123151+353929	12 31 51.76 +35 39 59.3	16.58	39	32	40	0.16	-0.01	
GB6J123350+502630	12 33 49.24 +50 26 23.4	17.44	283	175	64	0.39	0.83	
GB6J123413+475408	12 34 13.37 +47 53 51.6	17.21	356	268	176	0.23	0.39	
GB6J123417+505441	12 34 16.31 +50 54 25.7	16.94	66	48	41	0.26	0.26	
GB6J123532+522839	12 35 30.60 +52 28 28.1	17.44	88	80	68	0.08	0.14	
GB6J124036+695837	12 40 34.64 +69 58 31.2	17.50	133	190	164	-0.29	-0.12	
GB6J124307+731549	12 43 10.31 +73 16 00.9	14.20	493	312	153	0.37	0.65	
GB6J124313+362755	12 43 12.70 +36 27 45.1	17.41	148	91	53	0.39	0.57	
GB6J124732+672322	12 47 33.31 +67 23 16.8	16.65	264	174	131	0.34	0.39	
GB6J124818+582029	12 48 18.77 +58 20 28.8	15.80	245	356	324	-0.30	-0.16	
GB6J125311+530113	12 53 11.94 +53 01 12.1	17.13	488	363	366	0.24	0.16	
GB6J125614+565220	12 56 14.13 +56 52 23.8	12.81	318	415	256	-0.22	0.12	
GB6J130132+463357	13 01 32.61 +46 34 03.4	16.68	87	155	166	-0.47	-0.36	
GB6J130146+441612	13 01 46.35 +44 16 19.9	17.36	58	47	48	0.18	0.11	
GB6J130836+434405	13 08 37.90 +43 44 15.8	12.59	59	47	35	0.18	0.29	
GB6J130924+430502	13 09 25.58 +43 05 05.5	16.97	60	45	31	0.23	0.37	
GB6J131215+445023	13 12 16.81 +44 50 21.0	12.23	140	106	39	0.23	0.71	
GB6J131218+351522	13 12 17.75 +35 15 21.5	16.71	48	36	28	0.23	0.30	
GB6J131328+363538	13 13 27.28 +36 35 40.4	09.00	123	79	3	0.36	1.99	
GB6J131655+722619	13 16 58.95 +72 26 20.8	17.47	40	76	61	-0.51	-0.23	
GB6J131739+411538	13 17 39.18 +41 15 46.4	13.42	267	195	171	0.25	0.25	

Table 1 – continued

name	Position (J2000)	R mag	S _{1.4} (mJy)	S _{4.8} (mJy)	S _{8.4} (mJy)	$\alpha_{1.4}^{4.8}$	$\alpha_{1.4}^{8.4}$	flag
GB6J131947+514759	13 19 46.40 +51 48 06.7	17.39	1093	614	234	0.47	0.86	
GB6J132513+395610	13 25 13.34 +39 55 53.7	14.46	58	53	27	0.07	0.43	
GB6J134035+444801	13 40 35.25 +44 48 17.7	16.73	78	73	51	0.06	0.24	
GB6J134139+371653	13 41 38.81 +37 16 45.3	17.14	123	77	28	0.38	0.82	
GB6J134442+402811	13 44 41.55 +40 28 02.3	13.38	102	79	7	0.21	1.50	s (0.77)
GB6J134444+555322	13 44 42.21 +55 53 13.1	13.52	145	95	37	0.35	0.76	
GB6J134856+395904	13 48 55.95 +39 59 07.3	12.12	83	62	67	0.24	0.12	
GB6J134913+601114	13 49 15.29 +60 11 26.5	14.54	79	43	12	0.50	1.05	
GB6J134934+534125	13 49 34.72 +53 41 17.2	17.40	1097	644	764	0.43	0.20	
GB6J135251+654124	13 52 51.23 +65 41 14.1	17.10	129	70	79	0.50	0.28	
GB6J135313+350912	13 53 14.28 +35 08 48.3	16.26	43	31	28	0.27	0.24	
GB6J135327+401700	13 53 26.67 +40 16 58.8	10.91	41	35	32	0.13	0.14	
GB6J135607+413637	13 56 07.37 +41 36 14.9	16.90	27	40	38	-0.33	-0.20	
GB6J140850+650550	14 08 48.77 +65 05 28.3	17.44	35	43	48	-0.18	-0.18	
GB6J141132+742404	14 11 34.73 +74 24 29.4	17.35	107	82	73	0.21	0.21	
GB6J141159+423952	14 11 59.89 +42 39 48.9	17.15	92	50	45	0.49	0.40	
GB6J141343+433959	14 13 43.68 +43 39 45.5	16.06	49	39	27	0.18	0.33	
GB6J141536+483102	14 15 36.77 +48 30 30.6	17.43	42	37	39	0.10	0.04	
GB6J141946+542328	14 19 46.50 +54 23 15.1	15.53	814	1350	2247	-0.41	-0.57	
GB6J142312+505543	14 23 14.17 +50 55 38.7	16.65	309	232	214	0.23	0.21	
GB6J142814+391222	14 28 13.84 +39 12 18.4	17.47	252	169	138	0.32	0.34	
GB6J143120+395245	14 31 20.50 +39 52 41.8	16.73	219	259	235	-0.14	-0.04	
GB6J143239+361823	14 32 39.82 +36 18 08.2	13.50	119	137	88	-0.11	0.17	
GB6J143646+633645	14 36 45.68 +63 36 37.5	17.40	952	757	867	0.19	0.05	
GB6J143920+371148	14 39 20.52 +37 12 03.4	17.49	60	77	57	-0.21	0.02	
GB6J144920+422103	14 49 20.73 +42 21 01.3	17.23	156	118	96	0.23	0.27	
GB6J150411+685605	15 04 12.51 +68 56 14.8	17.18	133	227	112	-0.43	0.10	s? (0.55)
GB6J150522+604007	15 05 22.67 +60 40 13.3	15.69	56	35	3	0.39	1.64	
GB6J150854+373318	15 08 54.94 +37 33 28.3	15.34	15	39	<2	-0.79	>1.11	
GB6J150914+700436	15 09 13.02 +70 04 22.9	14.81	65	47	13	0.27	0.90	
GB6J151554+561850	15 15 56.27 +56 18 53.2	11.12	54	31	<2	0.44	>1.83	s (1.15)
GB6J151717+694715	15 17 14.61 +69 47 10.2	17.50	15	32	21	-0.64	-0.21	
GB6J151746+652456	15 17 47.55 +65 25 23.6	17.43	38	31	36	0.16	0.03	
GB6J151806+424346	15 18 06.20 +42 44 42.5	13.33	51	32	7	0.38	1.11	
GB6J151807+665746	15 18 08.95 +66 57 53.4	12.92	39	36	30	0.06	0.14	
GB6J151838+404532	15 18 38.93 +40 45 00.7	15.45	44	44	27	0.01	0.28	
GB6J152911+693455	15 29 14.41 +69 34 59.3	17.28	54	70	34	-0.22	0.26	
GB6J153134+720634	15 31 33.54 +72 06 41.4	17.50	419	444	232	-0.05	0.33	
GB6J153900+353053	15 39 01.66 +35 30 46.1	16.50	97	92	79	0.04	0.11	
GB6J153931+381011	15 39 32.11 +38 09 52.5	15.61	52	40	25	0.21	0.40	
GB6J154255+612950	15 42 56.94 +61 29 55.5	17.25	87	121	144	-0.27	-0.28	
GB6J154255+705000	15 42 55.44 +70 49 41.7	12.85	46	47	38	-0.02	0.10	
GB6J154504+525930	15 45 04.84 +52 59 26.0	17.48	208	122	64	0.43	0.66	
GB6J155158+580642	15 51 58.18 +58 06 44.8	16.70	191	348	305	-0.49	-0.26	
GB6J155722+544043	15 57 21.47 +54 40 20.0	13.64	114	85	48	0.24	0.48	s? (0.53)
GB6J155848+562524	15 58 48.30 +56 25 14.4	17.31	208	206	169	0.01	0.12	
GB6J155901+592437	15 59 01.67 +59 24 21.5	12.88	220	191	130	0.11	0.29	
GB6J155922+731026	15 59 28.95 +73 10 27.2	16.79	46	32	<2	0.29	>1.74	
GB6J160029+613743	16 00 29.53 +61 37 26.7	13.94	104	61	<2	0.43	>2.20	s (0.65)
GB6J160318+694552	16 03 18.49 +69 45 57.4	17.12	203	172	102	0.13	0.38	
GB6J160357+573101	16 03 55.95 +57 30 54.8	17.39	332	365	308	-0.08	0.04	
GB6J160532+531250	16 05 32.23 +53 12 59.5	14.66	63	43	26	0.31	0.49	
GB6J160820+601834	16 08 20.67 +60 18 29.5	16.67	62	59	35	0.04	0.32	
GB6J161447+374554	16 14 46.93 +37 46 07.4	16.68	50	36	67	0.26	-0.16	
GB6J161941+525617	16 19 42.44 +52 56 13.5	17.38	183	128	181	0.29	0.00	
GB6J161947+523319	16 19 45.99 +52 33 13.3	14.59	49	30	<2	0.40	>1.78	
GB6J162025+690512	16 20 26.29 +69 04 47.6	17.16	72	46	25	0.36	0.59	
GB6J162303+662411	16 23 04.44 +66 24 01.0	17.00	156	481	302	-0.91	-0.37	

Table 1 – continued

name	Position (J2000)	R mag	S _{1.4} (mJy)	S _{4.8} (mJy)	S _{8.4} (mJy)	α _{1.4} ^{4.8}	α _{1.4} ^{8.4}	flag
GB6J162308+390946	16 23 07.60 +39 09 32.4	16.62	180	244	219	-0.25	-0.11	
GB6J162509+405345	16 25 10.35 +40 53 34.4	12.21	164	110	86	0.32	0.36	
GB6J162612+512044	16 26 11.61 +51 20 39.3	17.30	50	35	21	0.29	0.49	
GB6J162636+580914	16 26 37.42 +58 09 11.7	16.50	534	315	157	0.43	0.68	
GB6J163801+552547	16 38 00.70 +55 25 25.2	13.61	164	107	5	0.34	1.92	
GB6J163813+572029	16 38 13.41 +57 20 24.2	17.09	1199	1750	1326	-0.31	-0.06	
GB6J164220+665608	16 42 21.79 +66 55 49.3	17.29	127	73	47	0.45	0.55	
GB6J164258+394842	16 42 58.77 +39 48 37.0	16.12	7099	8719	5439	-0.17	0.15	
GB6J164420+454644	16 44 20.05 +45 46 45.4	17.06	188	109	64	0.44	0.60	
GB6J164734+494954	16 47 35.13 +49 49 57.2	16.49	182	191	189	-0.04	-0.02	
GB6J165138+400227	16 51 37.64 +40 02 17.2	17.39	44	49	31	-0.10	0.19	
GB6J165353+394541	16 53 52.24 +39 45 36.6	11.50	1562	1375	2772	0.10	-0.32	
GB6J165414+434319	16 54 12.49 +43 43 10.6	17.50	85	46	16	0.50	0.93	
GB6J165503+540754	16 55 05.07 +54 07 57.2	16.50	50	31	7	0.38	1.09	
GB6J165547+444735	16 55 47.36 +44 47 25.0	15.15	38	35	37	0.07	0.02	
GB6J165721+570556	16 57 20.76 +57 05 54.5	17.40	940	764	521	0.17	0.33	
GB6J165728+741302	16 57 32.33 +74 12 51.3	16.99	8	51	62	-1.50	-1.14	
GB6J170123+395432	17 01 24.70 +39 54 36.2	17.27	191	150	285	0.19	-0.22	
GB6J170449+713840	17 04 47.05 +71 38 16.9	16.81	36	43	30	-0.15	0.10	
GB6J170716+453607	17 07 17.77 +45 36 11.7	17.45	795	461	319	0.44	0.51	
GB6J171523+572434	17 15 22.94 +57 24 40.5	11.26	58	35	26	0.40	0.44	
GB6J171613+683636	17 16 13.94 +68 36 38.3	17.37	489	838	819	-0.44	-0.29	
GB6J171718+422711	17 17 19.18 +42 26 59.6	16.00	134	125	81	0.06	0.28	
GB6J171813+422759	17 18 15.20 +42 28 19.2	17.24	112	86	62	0.21	0.33	
GB6J171914+485839	17 19 14.59 +48 58 49.3	13.76	146	164	206	-0.10	-0.19	
GB6J171937+480404	17 19 38.31 +48 04 12.2	16.20	64	109	188	-0.44	-0.60	
GB6J171941+354700	17 19 36.23 +35 47 06.0	17.41	34	30	<2	0.11	>1.59	
GB6J172110+354217	17 21 09.53 +35 42 16.5	17.18	821	784	601	0.04	0.17	
GB6J172315+654751	17 23 14.13 +65 47 46.1	16.99	239	182	166	0.22	0.20	
GB6J172535+585127	17 25 35.07 +58 51 39.3	17.12	76	55	49	0.26	0.24	
GB6J172722+551059	17 27 23.49 +55 10 53.9	17.31	144	274	265	-0.52	-0.34	
GB6J172818+501315	17 28 18.58 +50 13 11.3	15.68	228	145	161	0.37	0.19	
GB6J172859+383819	17 28 59.20 +38 38 26.6	17.27	242	219	187	0.08	0.14	
GB6J173047+371451	17 30 46.88 +37 14 55.0	17.18	102	78	68	0.22	0.23	
GB6J173234+712359	17 32 32.75 +71 24 03.9	14.29	182	187	<2	-0.02	>2.52	s (0.96)
GB6J173312+704632	17 33 12.89 +70 46 32.5	14.53	81	71	8	0.10	1.29	s (1.00)
GB6J173410+421933	17 34 13.53 +42 19 57.3	15.26	51	36	8	0.28	1.03	
GB6J174113+722447	17 41 22.62 +72 24 51.5	17.46	89	52	63	0.43	0.19	
GB6J174231+594513	17 42 31.96 +59 45 07.3	17.08	107	88	116	0.16	-0.05	
GB6J174455+554220	17 44 56.50 +55 42 16.6	12.39	707	562	305	0.19	0.47	
GB6J174832+700550	17 48 32.88 +70 05 51.6	16.93	736	715	572	0.02	0.14	
GB6J174900+432151	17 49 00.21 +43 21 51.8	17.49	281	321	284	-0.11	-0.01	
GB6J174914+595351	17 49 20.96 +59 53 10.9	15.00	116	63	<2	0.49	>2.27	
GB6J175041+395706	17 50 41.17 +39 57 00.3	14.50	42	38	30	0.08	0.19	
GB6J175041+585132	17 50 40.58 +58 51 20.9	15.02	63	35	9	0.48	1.09	
GB6J175045+370858	17 50 44.75 +37 09 34.3	16.50	48	35	13	0.26	0.73	
GB6J175131+471259	17 51 31.62 +47 13 23.0	17.15	48	49	30	-0.01	0.27	
GB6J175546+623652	17 55 48.36 +62 36 44.4	11.00	288	203	147	0.28	0.38	
GB6J175628+580708	17 56 29.19 +58 06 58.2	16.89	52	38	24	0.25	0.43	
GB6J175704+535153	17 57 06.74 +53 51 37.3	15.07	60	42	39	0.29	0.24	
GB6J175728+552309	17 57 28.37 +55 23 11.7	14.11	80	73	50	0.07	0.26	
GB6J175833+663801	17 58 33.41 +66 37 58.8	13.07	772	875	<2	-0.10	>3.32	
GB6J180132+440409	18 01 32.29 +44 04 20.6	17.23	727	1193	522	-0.40	0.18	
GB6J180228+481932	18 02 31.66 +48 19 40.9	16.50	20	33	29	-0.39	-0.20	
GB6J180557+574749	18 05 57.64 +57 47 46.5	17.00	89	48	12	0.50	1.12	s (0.66)
GB6J180651+694931	18 06 50.46 +69 49 28.1	15.06	2032	2122	1595	-0.04	0.14	
GB6J180738+563159	18 07 37.75 +56 31 56.8	15.50	25	32	13	-0.21	0.36	
GB6J181156+521431	18 11 57.12 +52 14 26.5	17.09	61	51	60	0.14	0.00	
GB6J181349+472123	18 13 50.19 +47 21 14.9	14.50	136	78	14	0.45	1.27	
GB6J181912+551103	18 19 10.12 +55 11 08.2	17.03	77	67	64	0.11	0.10	
GB6J181932+362230	18 19 32.87 +36 22 32.9	16.89	105	61	21	0.44	0.90	
GB6J183750+641842	18 37 50.06 +64 18 40.7	16.90	40	35	45	0.10	-0.07	
GB6J183850+480237	18 38 49.22 +48 02 35.0	17.37	30	41	32	-0.25	-0.03	

Table 1 – continued

name	Position (J2000)	R mag	S _{1.4} (mJy)	S _{4.8} (mJy)	S _{8.4} (mJy)	$\alpha_{1.4}^{4.8}$	$\alpha_{1.4}^{8.4}$	flag
GB6J183858+573535	18 38 58.66 +57 35 38.1	16.93	88	93	66	-0.05	0.16	
GB6J184033+621257	18 40 33.53 +62 12 49.5	16.50	67	72	65	-0.06	0.01	
GB6J184214+470952	18 42 15.26 +47 09 44.7	16.00	61	40	11	0.34	0.95	s (0.78)
GB6J184917+670548	18 49 15.90 +67 05 40.9	16.47	518	845	476	-0.40	0.05	
GB6J184941+642522	18 49 40.73 +64 25 15.4	15.00	74	47	13	0.37	0.97	
GB6J185328+504652	18 53 32.26 +50 46 12.3	16.50	34	31	6	0.07	0.97	s? (0.99)
GB6J185455+735112	18 54 57.41 +73 51 20.7	16.89	465	576	600	-0.17	-0.14	
GB6J185852+682747	18 58 55.20 +68 27 39.8	15.77	52	30	2	0.44	1.74	
GB6J190042+645242	19 00 46.13 +64 52 57.4	16.83	105	59	10	0.47	1.31	
GB6J190101+620727	19 01 03.11 +62 07 21.2	16.87	109	68	23	0.38	0.87	
GB6J191212+660826	19 12 07.38 +66 07 46.9	15.11	67	39	21	0.44	0.65	
GB6J192325+740407	19 23 23.05 +74 04 05.1	15.00	195	111	<2	0.46	>2.56	
GB6J192747+735755	19 27 48.53 +73 58 02.1	16.50	3951	3626	3697	0.07	0.04	
GB6J194553+705545	19 45 53.64 +70 55 48.3	17.12	953	677	482	0.28	0.38	
GB6J230115+351252	23 01 14.45 +35 13 00.6	16.83	90	129	109	-0.29	-0.11	
GB6J232349+365047	23 23 50.22 +36 51 04.2	14.96	71	68	24	0.03	0.60	
GB6J235352+385549	23 53 50.59 +38 55 54.9	17.08	48	31	20	0.36	0.49	

4.1 The steep spectrum sources

By definition, the CLASS sources have a flat spectrum between 1.4 and 4.8 GHz ($\alpha_{1.4}^{4.8}$, $S \sim \nu^{-\alpha}$) as computed from the NVSS and the GB6 fluxes. Making use of the 8.4 GHz mentioned above, a new spectral index was determined, this time between 1.4 and 8.4 GHz ($\alpha_{1.4}^{8.4}$). Figure 2 shows the distribution of $\alpha_{1.4}^{4.8}$ and $\alpha_{1.4}^{8.4}$ for the sample while Figure 3 shows $\alpha_{1.4}^{8.4}$ versus $\alpha_{1.4}^{4.8}$.

In general, the two indices are well correlated although a dispersion is clearly observed. If the steepest objects are excluded (i.e., those with $\alpha_{1.4}^{8.4} \geq 0.7$), the slope of the correlation is consistent with a one-to-one relationship. The dispersion of the points on this fixed one-to-one relationship is $\sigma_y=0.25$. Given this dispersion, it is expected that a number of objects will have a rather steep spectrum between 1.4 and 8.4 GHz, even if they were selected to have a flat spectrum between 1.4 and 4.8 GHz. More quantitatively, about 10 objects are expected to have $\alpha_{1.4}^{8.4} \geq 0.75$. The observed number, however, is much higher (60, including the lower limits) thus indicating that there is a clear “tail” of steep objects that cannot be explained simply as due to the statistical dispersion on the $\alpha_{1.4}^{4.8}/\alpha_{1.4}^{8.4}$ correlation. This “tail” is clearly visible also in Figure 2b.

The 60 sources with $\alpha_{1.4}^{8.4} \geq 0.75$ were submitted to further inspection of the NVSS maps and were gathered in 2 groups:

1) Objects showing a complex morphology, with 2 or more components on scales of 2'-4': 15 sources.

2) Objects not resolved in many components (45 sources). Some of these are extended at the NVSS resolution ($S_{int}/S_{peak} > 1.1$) and others are compact ($S_{int}/S_{peak} \leq 1.1$).

In case 1 the GB6 flux is expected to be the sum of most if not all the components observed in the radio maps. The 1.4 GHz flux, instead, is the sum of the fluxes within 70'' from the GB6 position, as previously explained. Hence, for sources with an extension larger than 70'' the most external components are not included in the computation of the 1.4 GHz flux. The resulting $\alpha_{1.4}^{4.8}$ is thus flatter than the $\alpha_{1.4}^{8.4}$ computed with the total fluxes. For this reason the

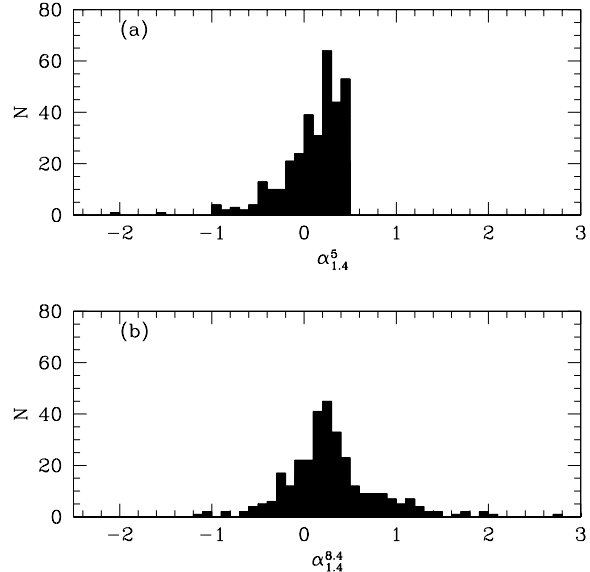


Figure 2. Distribution of the radio slopes between 1.4 GHz and 4.8 GHz (a) and between 1.4 GHz and 8.4 GHz (b). Both panels do not include lower limits

spectral index between 1.4 and 4.8 GHz was recomputed in these cases by adding all the components resolved in the NVSS maps and associated with the source itself. All sources turned out to have $\alpha_{1.4}^{4.8} \geq 0.5$ and they have thus been flagged as “steep” (an “s” in the flag column of Table 1; the corrected values of $\alpha_{1.4}^{8.4}$ are reported between parenthesis).

In case 2, the most probable reason for the observed steep $\alpha_{1.4}^{8.4}$ is that some flux is missed at 8.4 GHz. In fact, the VLA (A array) observations are expected to miss flux on scales larger than 6'' and, thus, well within the beamsize of the NVSS observations. This means that these objects are probably not strongly core dominated sources. The extreme example is the planetary nebula NGC 6543 (the object not detected at 8.4 GHz, GB6J175833+663801) which appears with $\alpha_{1.4}^{8.4} > 3$. This source is very strong at 1.4 GHz

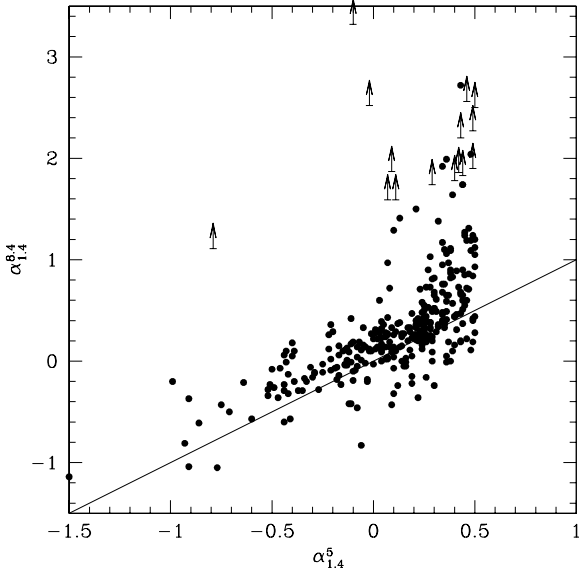


Figure 3. The spectral index between 1.4 and 8.4 GHz versus the spectral index between 1.4 and 4.8 GHz for the objects in the CLASS survey presented in this paper. The solid line represents the expected one-to-one relationship between the two indices; arrows correspond to lower limits based on the flux density detectability limits for the 8.4 GHz measurements.

(772 mJy) and at 4.8 GHz (875 mJy) but when observed at 8.4 GHz with a beam size of 0.24'', it disappears.

For reasons of completeness, the NVSS maps of the entire sample were inspected in order to identify all possible cases of sources that fall in case (1) studied above. This analysis revealed another 7 sources that were also flagged as "steep" (flag=s) in the last column of Table 1. (The NVSS maps for the 22 steep sources are shown in Figure 4.) It is interesting to note that the percentage of steep spectrum sources found in this sample corresponds exactly to that which is expected in the complete CLASS catalogue (Meyers et al. 2001).

In summary, the presence of a "tail" of some steep (between 1.4 and 8.4 GHz) sources is mainly due to the fact that at 8.4 GHz some flux is missed in objects which are not very compact.

4.2 The extended sources

Since 144 objects fall in the region of sky covered by the FIRST survey, it is possible to compute a reliable radio "compactness" parameter. The 16 objects which are resolved by FIRST in 2 components were excluded from the analysis.

Assuming:

$$S_{core} = S_{peak}^{FIRST}$$

and

$$S_{extended} = S_{total}^{FIRST} - S_{peak}^{FIRST}$$

the following parameter R is defined:

$$R = S_{core}/S_{extended}$$

In Figure 5 the computed R parameter versus $α_{1.4}^{8.4}$ is

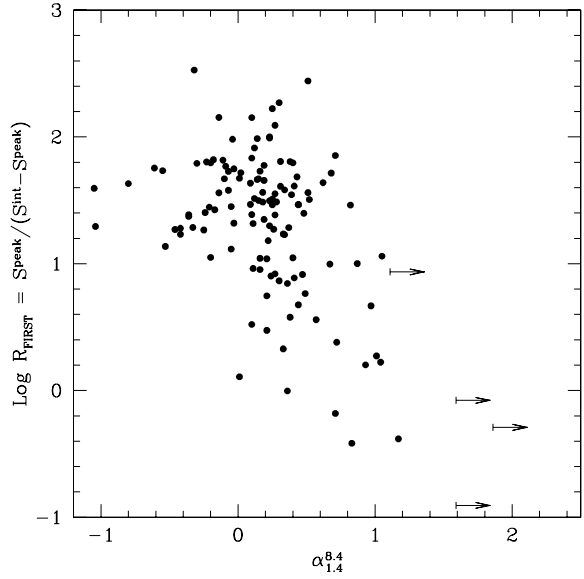


Figure 5. The radio "compactness" parameter (core/extended flux) defined with the FIRST fluxes assuming core flux=peak flux and extended flux=integrated – peak flux. The symbols are the same as in Figure 3

presented. Despite the large scatter observed in this plot, it is possible to infer the following conclusions: (1) the objects with a very flat (inverted) spectrum are all strongly core-dominated with $R \geq 10$; (2) the objects with steep spectrum ($α_{1.4}^{8.4} \geq 0.5$) cover a wide range of R parameter ranging from 0.1 up to 60 although the majority show $R \geq 1$. The extended sources are probably steep because at 8.4 GHz the VLA observations are missing a fraction of the extended flux (see discussion in the previous section). Nevertheless, the majority of sources with a steep $α_{1.4}^{8.4}$ are compact in the FIRST maps. For these, variability could be another possible explanation for the observed difference between $α_{1.4}^{8.4}$ and $α_{1.4}^{4.8}$.

5 CONCLUSION

A new deep sample of flat radio spectrum sources based on CLASS data has been presented. This sample has been designed to select and study the low-luminosity tail of the blazar class of AGN which, under the current unification model, should contain mainly optically featureless objects (BL Lacs). The goal is to test this hypothesis by systematically studying the optical properties of a well defined and complete local sample of blazars. To this end, only the optically bright ($R \leq 17.5$) CLASS sources have been considered. The resulting sample contains 325 objects and it is the natural extension of the 200 mJy sample by Marchā et al. (1996) down to fainter fluxes (30 mJy at 4.8 GHz).

In this first paper the radio properties of these 325 objects have been studied by using the available data at different frequencies and resolutions. It has been concluded that the vast majority of the objects selected in the CLASS blazar survey are compact ($R \geq 1$) even at the 6'' beam of the FIRST survey with a large percentage ($\sim 76\%$) of objects with very

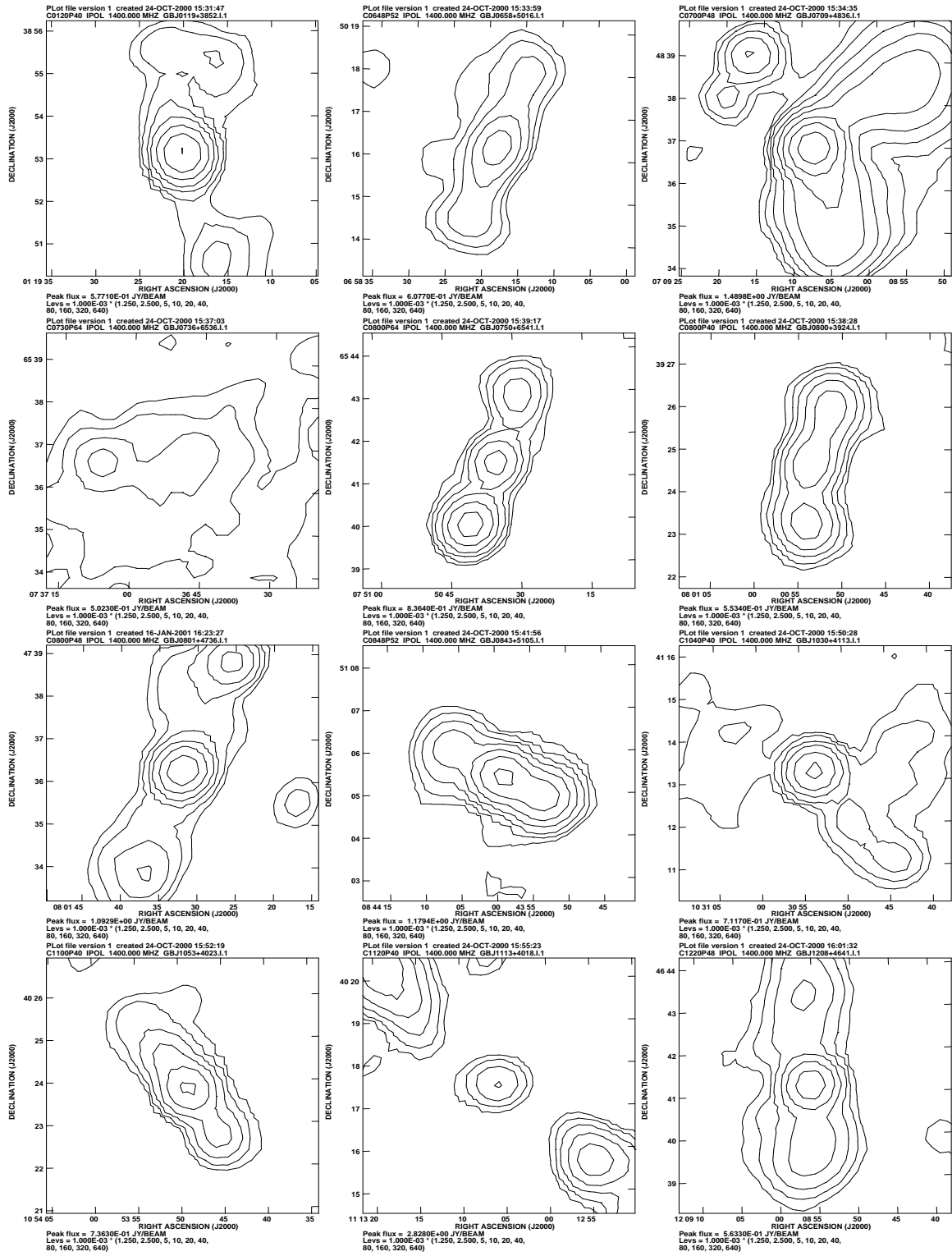
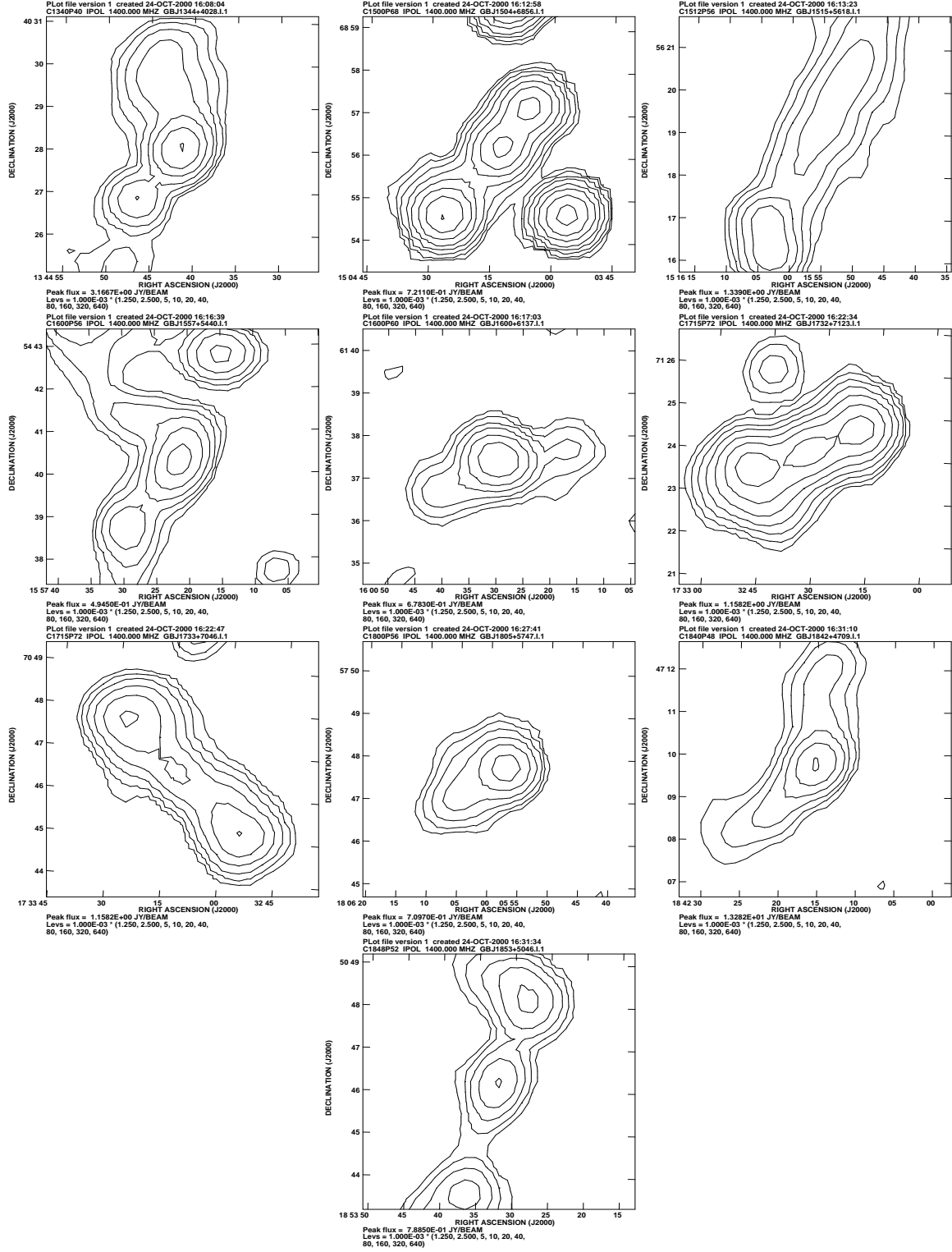


Figure 4. The NVSS maps of the lobe-dominated steep spectrum sources discovered in the CLASS sample

high R (≥ 10). Furthermore, it has also been shown that the spectral index between 1.4 and 4.8 GHz is well correlated with the index computed between 1.4 and 8.4 GHz. Finally, only 22 objects show clear lobe-dominated radio structures which owe their appearance in the sample to the different resolution of the catalogues used for the selection.

The optical follow-up of the entire sample is in progress and, so far, more than 70% of the objects have been spectroscopically classified. The results from the optical identification will be presented and discussed in a forthcoming paper (Caccianiga et al.; submitted to MNRAS).

**Figure 4 – continued**

ACKNOWLEDGMENTS

This research was supported in part by the European Commission Training and Mobility of Researchers program, research network contract ERBFMRX-CT96-0034 “CERES”.

REFERENCES

- Antón, S. 2000, PhD thesis, University of Manchester
 Becker, R.H., White, R.L., Helfand, D.J. 1995, ApJ, 450, 559
 Browne, I.W.A. & Marchā, M.J.M. 1993, MNRAS, 261, 795
 Condon, J.J. et al. 1998, AJ, 115, 1693
 Fossati, G., Maraschi, L., Celotti, A., Comastri, A., Ghisellini, G.

- 1998, MNRAS, 299, 433
Ghisellini, G. 1997, in Relativistic Jets in AGNs, ed. M. Ostrowski, M. Sikora, G. Madjeski, & M. Begelman (Krakow: Astron. Obs. Jagiellonian Univ.), p. 262.
Gregory, P.C., Scott, W.K., Douglas, K., Condon, J.J. 1996, ApJS, 103, 427
Jackson, N. & Marchā, M.J.M. 1999, MNRAS, 309, 153
Kühr, H., Witzel, A., Pauliny-Toth, I.I.K., Nauber, U. 1981, A&AS, 45, 367
Landt, H., Padovani, P., Perlman, E.S., Giommi, P., Bignall, H., Tzioumis, A., 2001, MNRAS, 323, 757.
Maraschi, L. & Rovetti, F. 1994, ApJ, 436, 79.
Marchā, M.J.M., Browne, I.W.A., Impey, C.D., Smith, P.S. 1996, MNRAS, 281, 425
Myers, S.T., et al. 2001, in preparation
Perlman, E.S., Padovani, P., Giommi, P., Sambruna, R., Jones, L.R., Tzioumis, A., Reynolds, J. 1998, AJ, 115, 1253
Taylor, G.B., Vermeulen, R.C., Readhead, A.C.S., Pearson, T.J., Henstock, D.R., Wilkinson, P.N. 1996, ApJS, 107, 37
Urry, C.M., Padovani, P. 1995, PASP, 107, 803.
White, R.L., Becker, R.H., Helfand, D.J., Gregg, M.D. 1997, ApJ, 475, 479
White, N.E., Giommi, P., Angelini, L. 1994, IAU Circ. 6100